A nanoindentation investigation of local strain rate sensitivity in dual-phase Ti alloys

Tea-Sung Jun[1,*], David E.J. Armstrong[2], T. Benjamin Britton[1]

[1]Department of Materials, Royal School of Mines, Imperial College London, London, SW7 2AZ, UK
[2]Department of Materials, University of Oxford, Parks Road, Oxford, OX1 3PH, UK

[*]Corresponding author. Email address: t.jun@imperial.ac.uk

Abstract

Using nanoindentation we have investigated the local strain rate sensitivity in dual-phase Ti alloys, Ti-6Al-2Sn-4Zr-xMo (x=2 and 6), as strain rate sensitivity could be a potential factor causing cold dwell fatigue. Electron backscatter diffraction (EBSD) was used to select hard and soft grain orientations within each of the alloys. Nanoindentation based tests using the continuous stiffness measurement (CSM) method were performed with variable strain rates, on the order of 10^{-1} to $10^{-3}s^{-1}$. Local strain rate sensitivity is determined using a power law linking equivalent flow stress and equivalent plastic strain rate. Analysis of residual impressions using both a scanning electron microscope (SEM) and a focused ion beam (FIB) reveals local deformation around the indents and shows that nanoindentation tested structures containing both α and β phases within individual colonies. This indicates that the indentation results are derived from averaged α/β properties. The results show that a trend of local rate sensitivity in Ti6242 and Ti6246 is strikingly different; as similar rate sensitivities are found in Ti6246 regardless of grain orientation, whilst a grain orientation dependence is observed in Ti6242. These findings are important for understanding dwell fatigue deformation modes, and the methodology demonstrated can be used for screening new alloy designs and microstructures.

Key words: Titanium alloys, strain rate sensitivity, nanoindentation, electron backscatter diffraction (EBSD), cold dwell fatigue

This is an authors' copy of a manuscript which has been accepted for publication in Journal of Alloys and Compounds.

1. Introduction

Titanium alloys are used extensively in aerospace applications where fatigue is one of the most significant issues to contend with and manage. In particular, the nature of modern flying now includes some significant holding at high load for extended periods, for instance between take-off and cruise [1], in order to maximise fuel efficiency and reduce noise pollution. Further load-holds occur during thrust reversal to land on short run ways. These regimes are cyclic (once or twice per flight) and have a time sensitive load hold, leading to concern regarding rate sensitive deformation modes involved in dwell fatigue.

Cold dwell fatigue has been a critical issue in aero-engine industry for the last few decades [1, 2]. Cold dwell susceptible alloys are those which suffer from a significant reduction in fatigue life due to the inclusion of a short load-hold (~120s) at low to moderate temperatures (up to ~200°C). This can reduce the number of cycles to failure by a decade or more and this is called the "dwell debit". In dual-phase Ti alloys (Ti-6Al-2Sn-4Zr-xMo), Mo content significantly affects dwell sensitivity, where Ti6242 is dwell sensitive and Ti6246 is not [3]. A chemical, structural or morphological effect has been thought of as a cause of dwell fatigue due to differences in β volume fraction and local chemistry between these alloys.

In practice, dwell fatigue failure is mitigated by use of dwell insensitive alloys and careful maintenance schedules, but management of this phenomena costs the aerospace industry significantly (~£100m / year). It is therefore important to understand microstructural contributions towards the dwell process to enable more cost effective component management strategies and ultimately engineering new materials that are dwell insensitive.

Recently it has been demonstrated that dwell fatigue failure is dominated by local microstructure in many dual-phase Ti alloys, including the presence of a rogue grain combination [4]; where, during the load-hold, stress is shed (i.e. redistributed) from a 'soft'

grain to a neighbour 'hard' grain in the Stroh model [2, 5]. Therefore local regions of very high stress form across the interface [6, 7]. Hard and soft grains here represent those grains that are poorly oriented for an applied deformation mode and appropriately oriented for easy slip (i.e. $\langle a \rangle$ type basal or prism slip) respectively. For titanium this is often described considering the angle between the $\langle c \rangle$ axis of the unit cell and principal loading axis, where applying a normal stress parallel to the $\langle c \rangle$ axis is a hard orientation and deforming perpendicular to the $\langle c \rangle$ axis is a soft orientation.

In dwell fatigue, time dependent stress amplification during this load shedding process at local microstructural regions near the interface is thought to play a predominant role in failure through facet formation [8]. Prior research indicates that the function of basal plane orientation is important in dwell fatigue for dual-phase Ti alloys [9-13]; yet fundamental deformation mechanisms within each hard and soft grain (i.e. contributions of individual slip systems) are still unknown.

One hypothesis on time sensitive dwell fatigue is that strain rate sensitivity (SRS) is a crucial factor governing the load shedding phenomenon. As titanium alloys are typically more elastically and plastically anisotropic at the grain scale [14-16], there are likely to be differences in the SRS of different grain orientations due to variable rate sensitivities of the different slip systems [17]. These slip systems are $\langle a \rangle$ dislocations on prismatic planes; $\langle a \rangle$ dislocations on basal planes; and $\langle c + a \rangle$ slip systems on pyramidal slip planes. Each slip system has a different critical resolved shear stresses, where their ratio is likely to be ~3:4:9 [18, 19]. Even though the $\langle c + a \rangle$ deformation mode has a significantly higher CRSS value it is still likely to activate, as slip with $\langle a \rangle$ type dislocations only does not provide 5 independent deformation modes which are required to accommodate an arbitrary shape change.

Nanoindentation has been previously used to study the mechanical response of single grains in titanium alloys. Quasistatic nanoindentation, combined with TEM of Ti-7Al, reveals that indentation into different grain orientations activates different slip systems [20]. In particular indentation into the basal plane activated both $\langle c+a \rangle$ type dislocations and $\langle a \rangle$ type dislocations. The $\langle a \rangle$ type dislocations were of opposite sign to the $\langle a \rangle$ component of the $\langle c+a \rangle$ dislocations to enable local deformation and support the local curvature around the indent. This supports a prior demonstration [21] that indentation into grains of Ti-6Al-4V revealed clearly that these mechanisms also happen in dual-phase microstructures and in particular that $\langle c+a \rangle$ type dislocations are geometrically required if twinning does not activate. This change in plastic deformation mechanism, when indenting into grains of different crystallographic orientation, results in significant anisotropic hardness measurements. Additionally indentation, combined with EBSD, has been used to systematically study grains of different orientations and confirmed that the anisotropic mechanical performance is consistently observed across a range of Ti alloys [14, 16, 22, 23]. Furthermore, experimental data has been fitted with crystal plasticity models has enabled extraction of the critical resolved shear stress for different dislocation types [14, 16].

The nanoindentation approach is insightful and relatively inexpensive to undertake, but precise mechanistic analysis is fraught with complications, as the stress state around the indention is complex and there are likely to be significant lengthscale contributions due to the indentation size effect for small indentation depths. Often these effects are considered for relatively isotropic materials, yet in HCP alloys ignoring the effect of orientation is likely to be problematic. This does not diminish from the potential use of nanoindentation to elucidate mechanisms and highlight opportunities for further study.

Moving beyond hardness (i.e. strength) and considering strain rate sensitivity is now possible with indentation, as new experimental approaches have been developed. Typically nanoindentation is used for exploring a deformation resistance (i.e. hardness and modulus of elasticity) on a local scale [24], and use of the continuous stiffness measurement (CSM) approach [25] enables continuous measurement of hardness with depth during indentation, through measurement of the phase change of an applied oscillation of the tip displacement and the measured response of the material. Recent work has highlighted that this CSM approach can be very valuable in performing variable strain rate testing and therefore accessing the strain rate sensitivity at a local scale, such as exploring the SRS of nanocrystalline and ultrafine-grained metals [26-30].

In practice, a power law constitutive equation is typically used to define the indentation-based SRS exponent (i.e. m value) as follows [28, 31-36]:

$$m_{nanoindentation} = \frac{d(\ln H)}{d(\ln \dot{\varepsilon}_{indentation})} \quad (1)$$

with further following relations, $\dot{\varepsilon}_{indentation} = \dot{h}/h$ and $H = P/A$, where h is the indentation depth, $\dot{h}$ the penetration rate, P the applied load, A the project area for indent (e.g. $24.5h^2$ for perfect Berkovich tip) and H hardness.

The SRS at the nanoscale [36, 37] and macroscale [38-41] of Ti alloys have been determined using either uniaxial tensile/compression or nanoindentation-based test with different methods (e.g. constant strain rate and strain rate jump test). Observed m values were within a range of 0.007~0.04 for CP-Ti [36-39, 41], 0.0185 for Ti-6Al and 0.01 for Ti6242 [40], where the m value of metallic materials is in general lower than 0.1 at room temperature [42]. Direct comparison across alloys from these studies is not possible as microstructural features, such as grain size, and testing method were not similar.

Within this work, we use the CSM technique due to its fairly-straightforward experimental setup and data analysis. We note that there are some significant limitations that must be considered with this approach [28, 43], such as: (i) indentation data are sensitive to microstructure; (ii) thermal drift may play a prominent role at lower strain rates (i.e. longer testing time); and (iii) significant experimental error can be occurred in soft metallic materials (e.g. single crystal) with a large E/H ratio. Recently several authors have reported [28, 44-46] using a modified CSM method to study SRS effects on hardness by utilising step changes in load rate in a single indentation. This has the advantage that a single indentation can be utilized to study the effect of rate sensitivity on hardness and this can also overcome issues with environmental instabilities leading to thermal drift artefacts in very slow strain rate indentations. However, while the modified CSM method has been shown to work well on monocrystalline metals there are issues with interpretation of the data on coarser grained materials. This is especially important when there are significant indentation size effects [47] that lead to an increased hardness as a function of indentation depth, superimposed on-top of any change in hardness due to strain rate changes. Secondly the hardness change measured is by definition taken at points where differing volumes of plastic deformation have occurred. In nanocrystalline materials this is not of concern as the 'length scale effects' are linked to the nano-grain sizes, rather than the indentation volume. However in other microstructures this can lead to comparing hardness changes which are controlled by both sampling differing microstructures, e.g. due to heterogeneity or length-scale effects under the indenter impression, as well as strain rate changes.

While nanoindentation approaches can clearly measure different rate sensitivities during deformation, care must be taken in interpretation, as comparison with more conventional engineering measures of strain rate sensitivities is difficult because the local strain field around the indenter during each test is rather complex [14, 48]. Here, we describe rate

sensitivity (i.e. equivalent to SRS obtained from uniaxial tensile or compression test) as the material response to the variable indentation rate. We use nanoindentation to provide a relatively simple and inexpensive method of testing multiple individual microstructural units in complex alloys at an appropriate lengthscale.

In this work, we investigate local rate sensitivity in dual-phase Ti alloys with a nanoindentation CSM method using multiple indentations at differing strain rates. This aims to provide a mechanistic insight on how the rate sensitivity varies with respect to crystal orientations (i.e. hard and soft grain). We focus on this as dwell fatigue has a time-sensitive load-hold and different orientations are important for the rogue grain combination within the Stroh model.

2. Experimental procedures

The Ti6242 (Ti-6Al-2Sn-4Zr-2Mo) and Ti6246 (Ti-6Al-2Sn-4Zr-6Mo) samples studied were supplied by IMR (Institute of Metal Research, China) as forged bars (details of the chemical composition are seen in Table 1). The bars had been produced by a triple VAR melt, followed by β forging and α-β forging. These samples were subsequently heat treated to create two similar samples with large α colonies. Samples sectioned perpendicular to the bar axis were heat-treated (Figure 1) at the temperature of β transus + 50°C (i.e. 1040°C for Ti6242 and 990°C for Ti6246) and cooled down with a sufficiently slow rate of 1°C/min, resulting in fully lamellar microstructure and minimal internal strain gradients.

Table 1. Chemical composition of Ti6242 and Ti6246

Samples	Al	Sn	Zr	Mo	C	Fe	Si	H	O	N
Ti6242 (wt. %)	6.08	2.00	3.95	2.00	0.012	0.031	0.021	0.0002	0.072	0.0069
Ti6246 (wt. %)	6.12	2.02	4.03	6.00	0.011	0.035	0.049	0.0005	0.068	0.0044

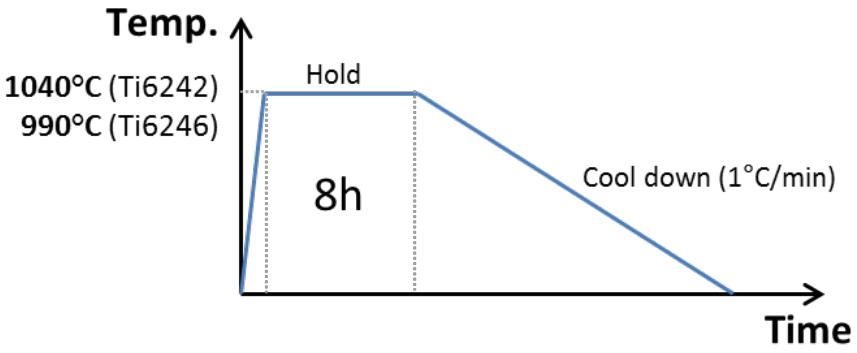

Figure 1. Schematic diagram of heat treatment (HT) processing route by holding at β transus + 50°C (i.e. 1040°C for Ti6242 and 990°C for Ti6246) for ~8h and cooling down with a rate of 1°C/min for ~17h.

The samples were ground with a series of SiC papers (up to 4000 grit) and subsequently polished with OP-S (Oxide Polishing Suspensions) diluted with H_2O (by a ratio 1:5 of OP-S:H_2O). Light surface etching was conducted with Kroll's reagent, a mixture of 2% HF, 10% HNO_3 and 88% H_2O. This chemically removes surface damage and provides very slight contrast for correlative optical microscopy, SEM, EBSD, FIB and nanoindentation experiments [49].

EBSD measurements were carried out in a Carl Zeiss Auriga CrossBeam FIB-SEM with Bruker eSprit v1.9 software, using a probe current of 10.5nA, an aperture size of 120µm and an accelerating voltage of 20kV. Large area maps were taken with step sizes of 4µm for Ti6242 and 2.2µm for Ti6246 (the step size was varied due to different phase volume fractions). Hard and soft colony regions were identified within each sample. Further small area maps were taken after the indentation experiments, with finer step sizes of 0.2µm, in

order to regularly reveal both α and β phase orientations and verify misorientation between the two phases within each colony.

Indentation experiments were carried out using the continuous stiffness measurement (CSM) technique [34, 43] using a NanoindenterXP (MTS, now Keysight). The CSM technique enables the contact stiffness to be continuously obtained as a function of depth by superimposing a small sinusoidal oscillation on the force signal and measuring the displacement response at the same frequency [43, 50]. The area function for this tip was calibrated using indentation into a fused quartz standard sample.

The strain rate sensitivity of each colony region was evaluated using a total of sixteen well-spaced indents. Arrays of 2000nm deep indents were created by a diamond Berkovich indenter, and CSM measurements were made with a 2nm amplitude and 45Hz oscillation. Indents were made for four target indentation strain rates of $2x10^{-1}$, $5x10^{-2}$, $5x10^{-3}$ and $1x10^{-3}s^{-1}$. For each region and strain rate, four repeat indents were made. Indents made at each strain rate were compared and showed similar results, indicating that these indents were representative of the indentation response of each microstructural region, and therefore data for each strain rate was averaged within TestWorks (the individual indentation data is provided in the data associated with this paper).

After indentation, imaging of the indentation arrays was performed with SEM, as well as imaging and FIB-cross sectioning, using a Zeiss Auriga CrossBeam instrument. FIB trenches normal to the sample surface were cut to reveal the subsurface microstructure in order to understand the nature of slip transfer as the indentation volume expands. Imaging was performed with the SEM to reveal subsurface lath morphology within the colony structure.

3. Results

We focussed on grain hard and soft grain orientations from both Ti6242 and Ti6246, as the local load shedding process near the interface of a rogue grain combination is thought to play a principal role in facet formation [8]. Figure 2(a) and (b) show the crystal orientation maps of heat-treated Ti6242 and Ti6246, respectively, with inserts of the crystal orientations and the associated Euler angle (φ_1, ϕ, φ_2) of α phases. These maps were searched for colonies which are hard (labelled H) and soft (labelled S), based upon evaluation of the ϕ angle that describes the angle between the $\langle c \rangle$ axis and the sample surface normal in Bunge convention. This indicates that each grain from both alloys is highly comparative in terms of the ϕ angle with 85° vs. 86° for soft grains and 17° vs. 17° for hard grains.

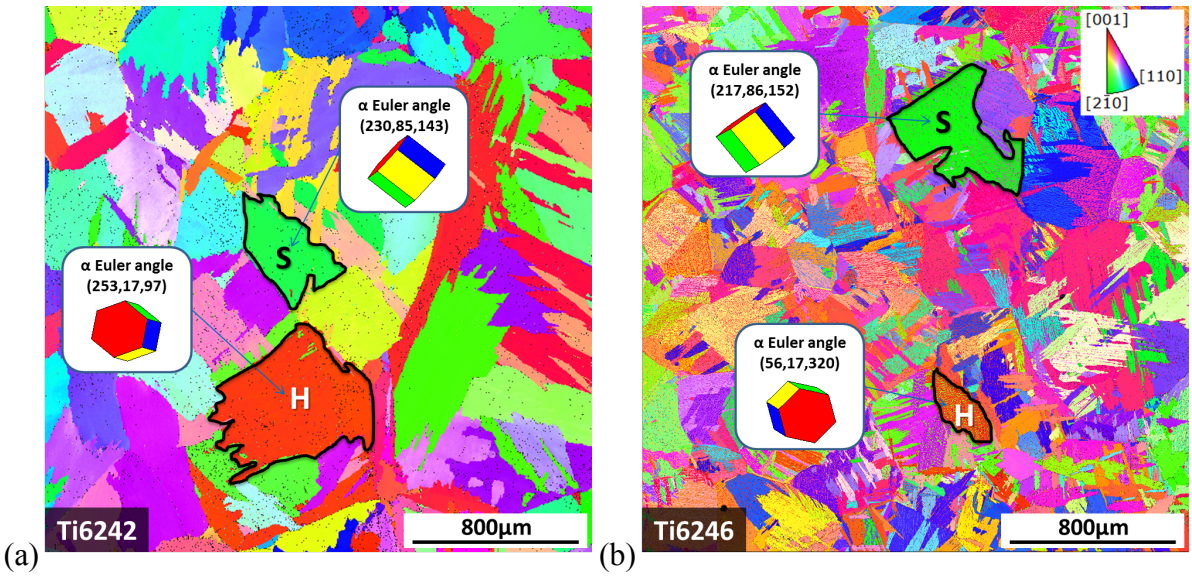

Figure 2. EBSD derived inverse pole figure (IPF) maps of (a)Ti6242 and (b)Ti6246, with inserts showing the crystal orientation of α phase and the associated Euler angle: The maps were taken with respect to the sample surface normal. H and S symbols marked within the regions indicate hard and soft grain, respectively.

Figure 3 shows the secondary electron (SE) micrographs captured after indentation tests. All sixteen indents were successfully made within the target colonies and were well separated.

The volume fractions of α and β phases in each of the alloys were determined through analysis of SE micrographs with ImageJ software (segmenting based upon image intensity)

[51]. In Ti6242, the two grains have similar volume fractions of about 0.90 for α and 0.10 for β phase, but different morphologies with long straight β ligaments for the hard grain and more wavy and divergent β ligaments in the soft grain. In Ti6246, the two grains have quite similar surface morphology and the volume fractions of about 0.55 and 0.45 for α and β phase, respectively.

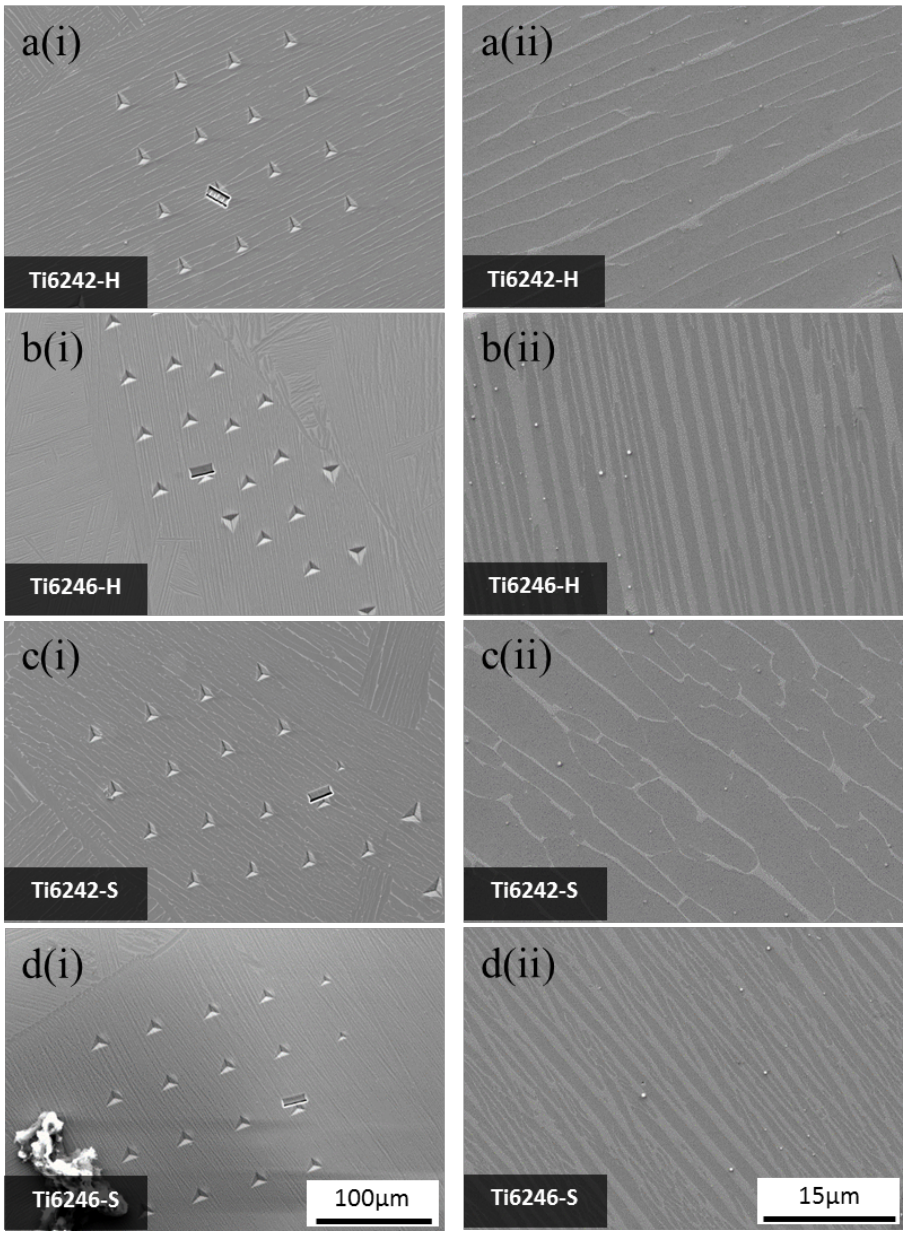

Figure 3. Secondary electron micrographs showing a(i)~d(i) indentation arrays, with α/β morphology and cross sectioned indentations highlighted and a(ii)~d(ii) high resolution images of each grain. The α phase is the dark phase and β is brighter; Contrast analysis reveals volume fractions of α and β (α:β) are 0.90:0.10 for Ti6242 and 0.55:0.45 for Ti6246.

Indents for each of the four target indentation strain rates showed good reproducibility within each colony. In Figure 4, one set of (depth dependant, CSM based) hardness measurement from each strain rate is presented for the different grain orientations and different materials. There is a limited apparent indentation size effect after ~750nm. It is seen that the hardness decreases mostly with decreasing strain rate, as expected, though there is a discrepancy at a rate of $5x10^{-3}s^{-1}$ in Figure 4(c).

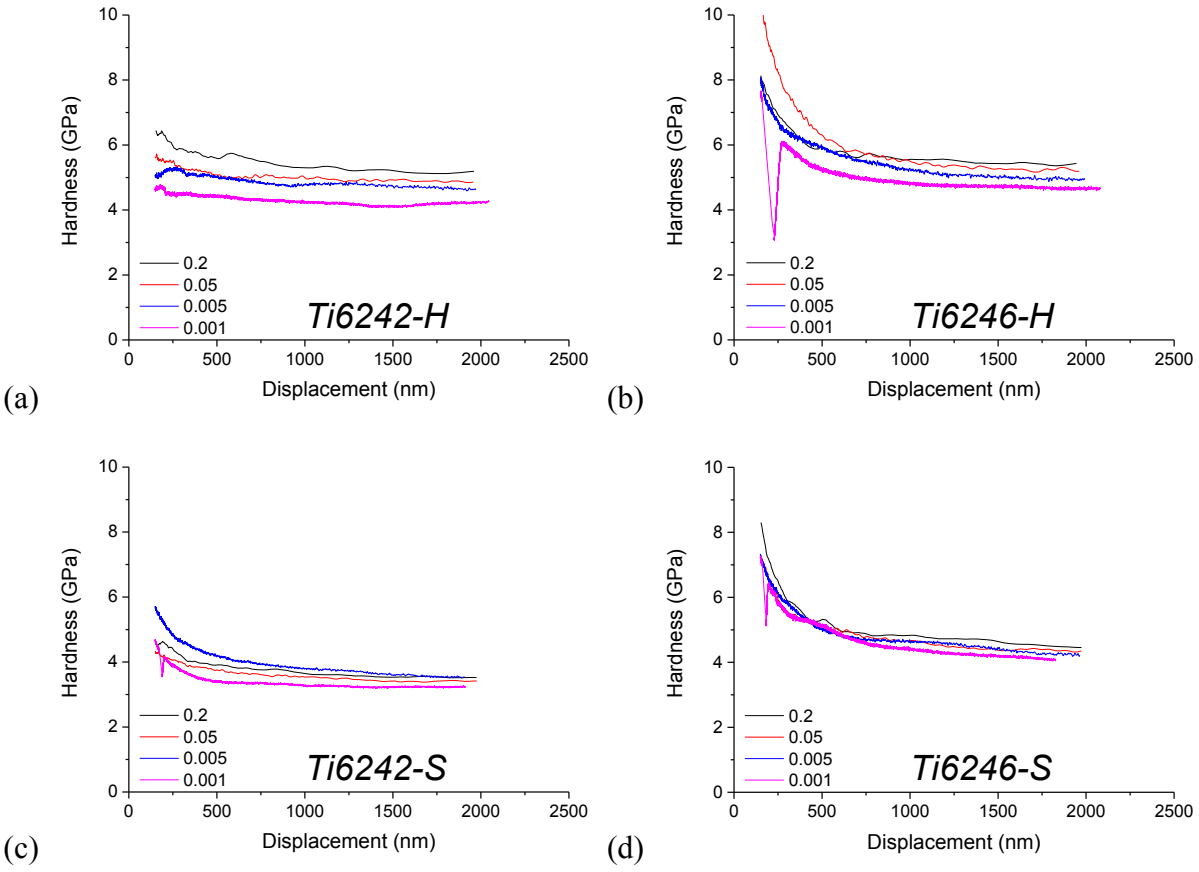

Figure 4. Individual hardness vs. displacement curves for both hard grains in (a) Ti6242, (b) Ti6246 and soft grains in (c) Ti6242, (d) Ti6246, showing an increase of hardness with increasing strain rate in general.

The average hardness values, for depths between 750 and 1750mm, were used to evaluate the rate sensitivity exponent (i.e. *m* value), in accordance with the Equation (1). Figure 5 shows plots of hardness against strain rate for the *m* value evaluation, on log-log plots. In Ti6246 the strain rate sensitivity is ~independent of grain orientation, with similar *m* values for hard and soft grains (0.022 and 0.028 respectively). In Ti6242 the strain rate sensitivity is strongly

dependant on grain orientation, with different *m* values for hard and soft grains in Ti6242 (0.039 and 0.0053 respectively).

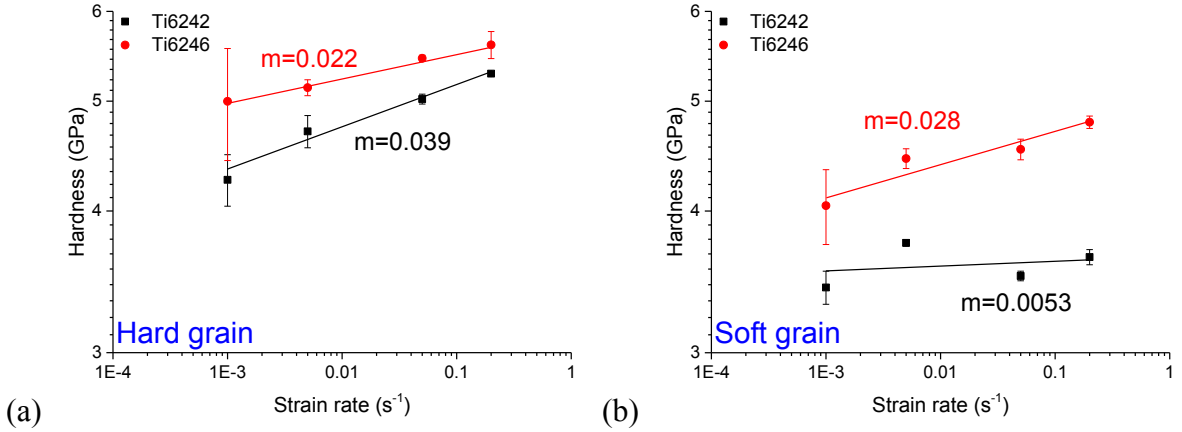

Figure 5. Hardness vs. strain rate (log-log form) in (a) hard and (b) soft grains of Ti6242 and Ti6246: a slope of each fitted line indicates the rate sensitivity exponent, m value.

The nanoindentation response for hard and soft orientations in Ti6242 and Ti6246 is markedly different. This motivated the SEM and FIB-SEM characterisation of the indented microstructure to aid understanding of these rate sensitivity results.

The local crystal orientations within each colony were examined in the hard grains of both samples (Figure 6(a)) with pole figures of α- and β-Ti. It reveals that Burgers orientation relationship (BOR) [52] is obeyed, where common poles were observed by overlapping poles in $\{0001\}_\alpha$ & $\{110\}_\beta$ and $\langle 11\bar{2}0\rangle_\alpha$ & $\langle 111\rangle_\beta$ [53, 54]. Identification of the common planes and directions enables determination of c-, a_1-/b_1- (closely aligned) and a_2-/b_2- (next most closely aligned) directions (shown in blue, green and yellow, respectively) based on the misorientations between Burgers vectors (i.e. a_1, a_2, a_3 and b_1, b_2) [7, 55].

The residual impressions of the indents show that the plastic zone surrounding each indent includes significant numbers of both α lamella and β ligaments in a composite structure (Figure 6(b)). Using the linear intercept method, α lamella and β ligament average widths

resulting of ~2.3μm and ~0.3μm for Ti6242 and ~1.0μm and ~0.7μm for Ti6246 were measured in this surface section.

Slip traces observed in these surface micrographs (round-dotted lines shown in Figure 6(b)) are analysed using superposition of the slip plane normal for basal, prismatic and pyramidal planes. Unfortunately it is rather difficult to confirm which slip systems were activated in this orientation, since the poles from each of those planes are interrogated only considering surface slip traces. The slip traces span from one α lamella to another, across a β ligament, for all three lobes around the indentation impression. The slip traces are clearly interrupted at the interface, indicating that slip transfer mechanisms at this interface are likely to play a role. Typically, the surface slip traces within both colonies are broadly similar in morphology, indicating that similar slip mechanisms are active in both materials.

From each array, the sub-surface structure of the colony was revealed with a FIB trench (see Figure 3), and the associated subsurface are seen in Figure 6(c). The colony structure for Ti6242 and Ti6426 are very similar in inclination with respect to the surface normal, allowing comparisons of the relative deformation of these two colony regions to be made.

Analysis of the soft orientation for each alloy is repeated in Figure 7. Again, the crystallography of each of the two phases obeys the BOR. In this colony, the α lamella and β ligament average widths were ~3.4μm and ~0.4μm for Ti6242 (rather different to the hard grain orientation) and ~1.0μm and ~0.8μm for Ti6246 (comparable to the hard) in the surface projection. Unlike slip traces in the hard grain orientations, surface slip traces obviously show activity of $\langle a \rangle$ slip on the prismatic plane. Here the slip traces tend to extend more continuously between α lamella and β ligaments, with clear surface steps in both phases. The subsurface microstructure between both alloys again has a similar inclination with respect to the indentation axis.

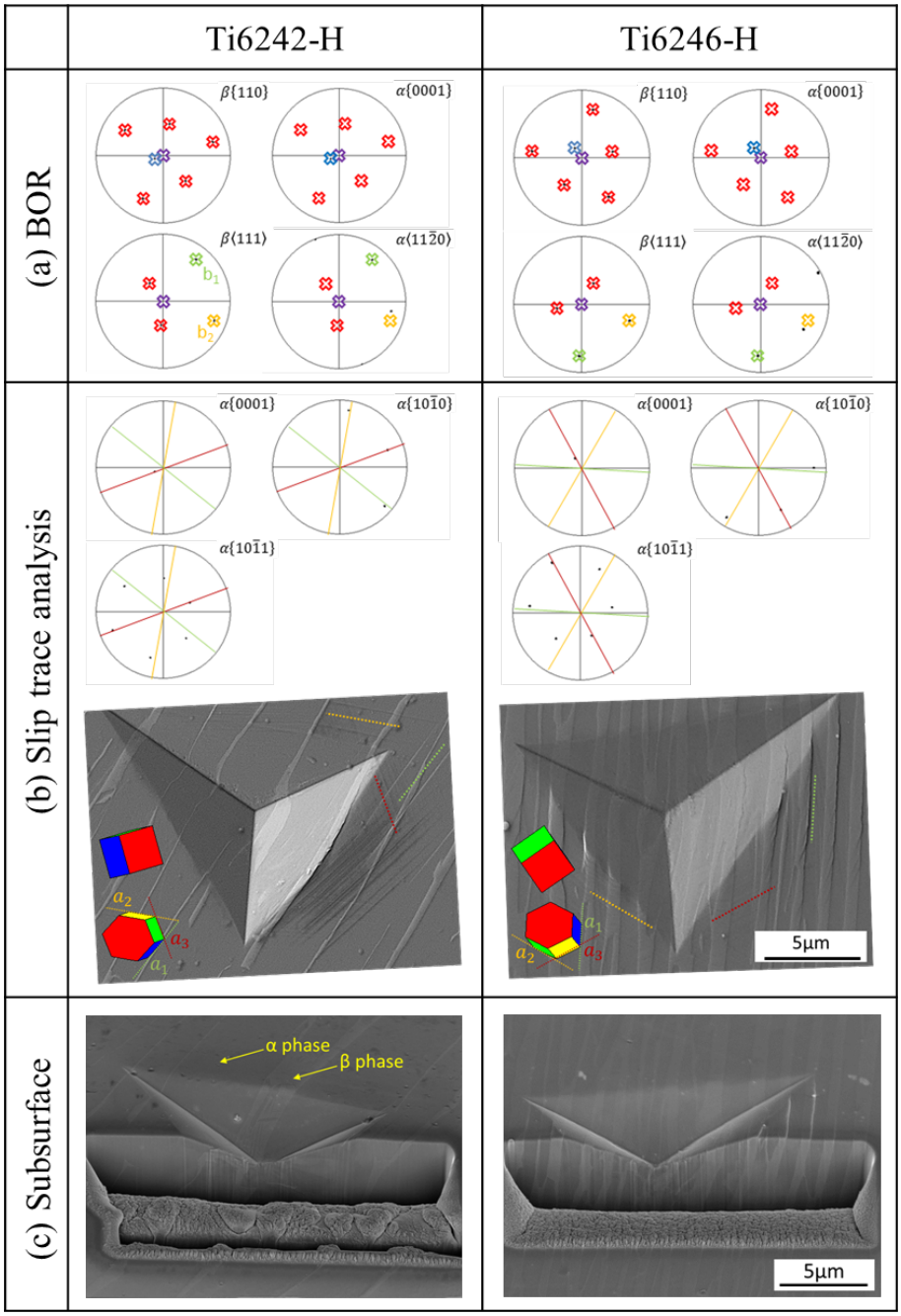

Figure 6. In hard grains of Ti6242 and Ti6246, (a) Pole figures of α- and β-Ti, indicating an obedience of Burgers orientation relationship (BOR): The purple cross represents the loading direction. For the crystal direction figures, the green and yellow crosses indicate a_1-/b_1- and a_2-/b_2- directions respectively. For the crystal plane figures the blue crosses represent the shared (0001)//(110) plane, (b) residual impression with inserts of crystal orientations of α and β phases (showing slip bands activated during indentation) and pole figures with overlapping solid lines of slip traces normal: The round-dot lines in green, yellow and dark red are parallel to the corresponding ⟨a⟩ directions (shown in the crystal orientations), (c) secondary electron micrographs taken at indented and its sub-surface areas in each region, showing α/β colony structure on the surface and underneath of the regions and slip bands: a trench was made by focused ion beam (FIB). (For interpretation of the references to colour in this figure legend, the reader is referred to the web version of this article).

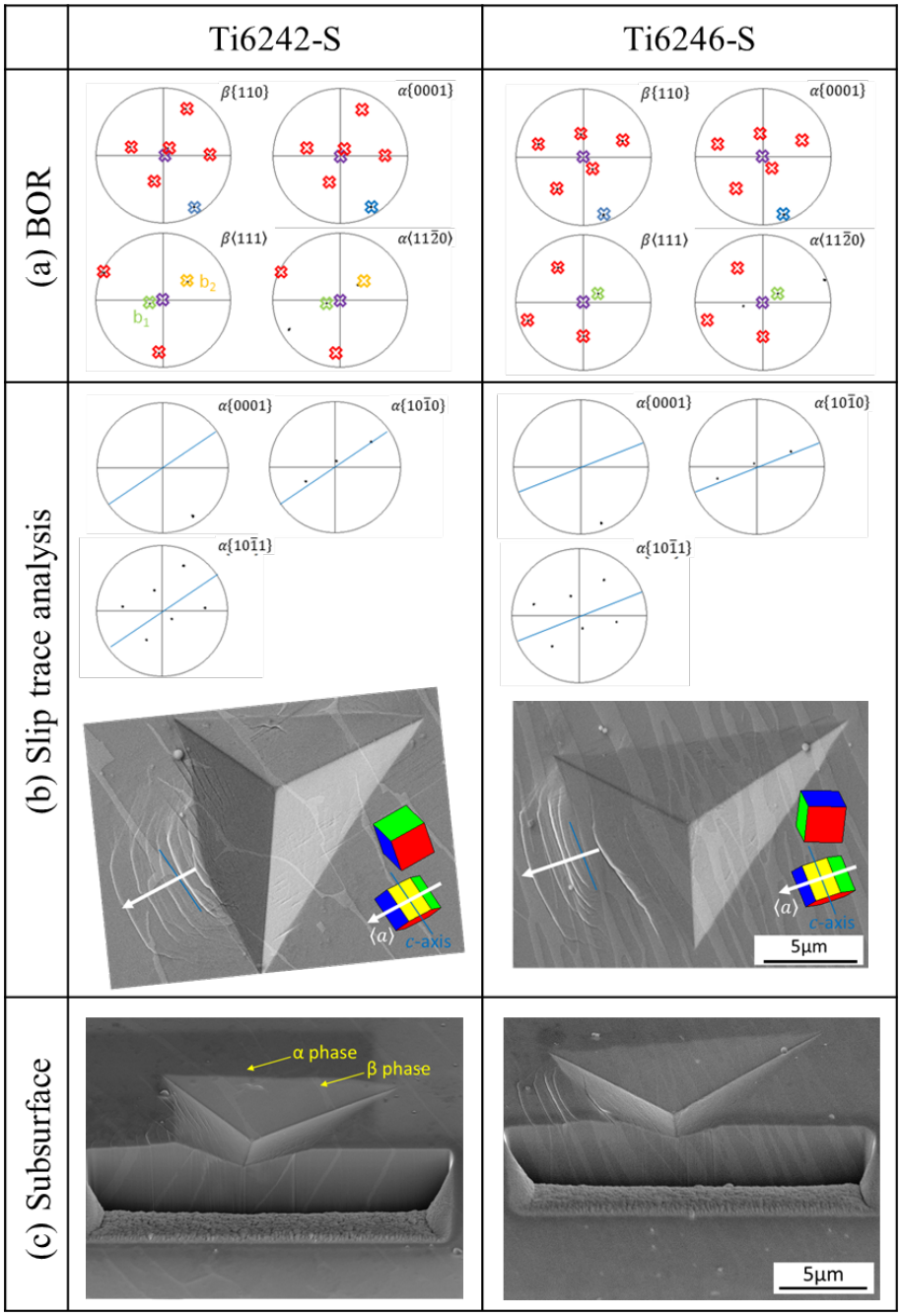

Figure 7. In soft grains of Ti6242 and Ti6246, (a) Pole figures of α- and β-Ti, indicating an obedience of Burgers orientation relationship (BOR): The purple cross represents the loading direction. For the crystal direction figures, the green and yellow crosses indicate a_1-/b_1- and a_2-/b_2- directions respectively. For the crystal plane figures the blue crosses represent the shared (0001)//(110) plane, (b) residual impression with inserts of crystal orientations of α and β phases (showing slip bands activated during indentation) and pole figures with overlapping solid line of slip traces normal: The white arrows indicate a direction perpendicular to the c-axis lined in blue, (c) secondary electron micrographs taken at indented and its sub-surface areas in each region, showing α/β colony structure on the surface and underneath of the regions and slip bands: a trench was made by focused ion beam (FIB). (For interpretation of the references to colour in this figure legend, the reader is referred to the web version of this article).

4. Discussion

In this study we have exploited new nanoindentation testing strategies to isolate the performance of individual microstructural units (colonies) and comparatively explored the orientation dependant rate sensitive response of two α+β titanium alloys. Correlating indentation with EBSD, SEM and FIB-SEM sectioning enables us to be confident that we have targeted a comparative microstructural region in two different engineering alloys with variable dwell sensitivities. This provides a comparative investigation of relative dwell sensitivity, through indentation *m* value determination, and enables down-selecting of alloys for further testing.

The most striking finding within this study is that, Ti6242 has higher rate sensitivity (m=0.039) for the hard orientation as compared to the soft orientation (m=0.005), whereas Ti6246 has comparable rate sensitivities for the hard and soft orientations (m=0.025). An important remark at this point is that interpreting those numbers and correlating directly to the load shedding phenomenon is not possible yet, as the numbers is likely to vary according to the testing methodology (i.e. tools, method) [28, 56-59]. However, we can argue with this comparative rate sensitivity study that dwell sensitive Ti6242 is orientation dependent rate sensitive and dwell insensitive Ti6246 is orientation independent rate sensitive. This has significant consequences when interpreting the behaviour of hard and soft microstructural regions (macrozones [60], microtextural regions [61] or effective structural units [62]) in the understanding of dwell fatigue for titanium alloys. This necessitates a revisit to the constitutive laws used to describe slip, where the slip rate sensitivity as well as the critical resolved shear stress may vary between slip systems within such models.

The nature of exploring real alloys, all-be-it with simplified microstructures, means that there remain some significant remaining hypotheses that need to be understood through further investigation in light of our findings:

(1) Does the volume fraction of β phase affect rate sensitivity?

As shown in Figure 3, the Ti6246 in this microstructural condition has a larger β volume fraction (~45%) than Ti6242 (~10%). This generates different volume fraction of interface between α and β phase, and the influence of the interfaces is likely to be important. The crucial aspect here is that the volume fraction variation is consistent (i.e. no or little interface effect) for both the hard and soft colonies in each alloy. The rate sensitivity of each colonies were directly compared and showed quite different trend. While this could be significant, it is not likely to be the only controlling microstructural feature and is likely to be a second order contribution to differences in rate sensitivity.

(2) Does the β ligament thickness affect rate sensitivity when slip transfer is 'easy'?

The soft colonies in both alloys will enable slip to progress relatively easily through the β ligaments, as the $\langle a \rangle$ type slip can progress through the β phase relatively easily due to the BOR. This can be elucidated by the slip trace analysis in Figure 7(b), such that indentation into soft colonies would activate $\langle a \rangle$ type slip in the α phase. The presence of the BOR means that some $\langle a \rangle$ type slip can be well aligned with slip systems in the β phase. This results in three alignments of the $\langle a \rangle$ type slip systems [17], where briefly the best aligned $\langle a \rangle$ slip system can be accommodated directly across into the β phase, which is called $\langle a_1 \rangle$ slip; the next is misaligned by ~10° between the $\langle a \rangle$ slip system in the α phase and the $\langle 111 \rangle \{110\}$ in the β phase and called $\langle a_2 \rangle$ slip; and the third is misaligned and is called $\langle a_3 \rangle$. $\langle a_1 \rangle$ and $\langle a_2 \rangle$ can result in direct slip transmission across the interface as they are reasonably well aligned with slip systems within the β phase. $\langle a_3 \rangle$ requires slip transfer to be accommodated by

collaborative sources and slip systems in the two phases and likely results in more dislocation locking, debris accumulation and time dependant mechanisms. For the hard colonies (see Figure 6(b)), principally the axial indentation strain must be accommodated by $\langle c + a \rangle$ slip or twinning. Neither of these two mechanisms are well accommodated through the β phase and are likely to result in significant hardening/slip interruption by the α/β interfaces, this makes transfer significantly more difficult.

For this soft colony orientation the Ti6246 contains significantly wider β ligaments (than the Ti6242), and the rate sensitivity of the Ti6246 is ~five times the rate sensitivity of the Ti6242. This hints strongly that either the β morphology or local chemical effects could be contributing to rate sensitive behaviour.

(3) Does the composite nature of the stacked α/β lath structure result in significant differences in strain accommodation, and therefore rate sensitivity, or is it instead related to the local crystallographic misorientation (and thereby effective slip length and dislocation transmission mechanisms)?

Compared to the Ti6246 showing comparable surface morphology (i.e. lath structures) between the targeted regions and β ligament thickness of 0.7~0.8μm, the Ti6242 revealed different lath structures (i.e. long straight ligaments for the hard grain and more wavy and divergent ligaments in the soft grain) and much thinner β (0.3~0.4μm). We note that these structures are two dimensional slices through complex 3D composite microstructures and a complicated deformation field surrounds each indentation. However the major deformation axis that controls the performance of these alloys is likely to be the indentation axis and therefore presentation of the colony widths with respect to this axis is probably a principal microstructure – deformation correlation. The difference in lath structures is therefore likely to be important. This is especially true when there is no easy slip transfer mechanism, such as

$\langle a_3 \rangle$ slip, through the interface, and instead elastic equilibrium and compatibility drives the progress of local deformation.

Studies have shown that $\langle a \rangle$ slip systems adjacent to β laths have significant anisotropic behaviour in dislocation pile-ups and transmission mechanisms at the α/β interface [17, 63, 64]. Relative slip transfer difficulties could be used to explain how two phases in a packet structure would result in very significant differences in the strain rate sensitivity for hard and soft grains. However, relative isotropy of the strain rate sensitivity of Ti6246 compared with Ti6242 (which both have a similar 'number' density of interfaces) renders this argument insufficient to describe the marked difference in rate sensitivity.

Consideration of our findings in light of these three mechanisms means that there must be a combined effect, whereby influence of the volume of the β packets together with activation of particular slip systems is likely to control the strain rate sensitivity of slip in these alloys. In practice, the presence of a rate sensitive mechanism may potentially change the structural unit size and therefore the grain size when considering dwell fatigue strength and component life. Mechanistically this will alter the effective slip length and the number of dislocations in a pile-up, required for the Stroh model of load shedding and stress amplification during dwell leading to facet formation and ultimately component failure [65, 66].

Our study outlines an initial first screen of the microstructural response and indicates that the next steps could either be: (1) local microstructural testing using a more confined stress state, e.g. with micropillar compression [49] or microcantilever deflection [67]; (2) thermomechanical processing to generate similar morphology microstructures for the Ti6246 alloy to make a Ti6242 like microstructure and verify if the strain rate sensitivity is controlled explicitly by morphology, rather than chemical effects of the Mo which is likely partitioned to the β phase.

This work complements previous work using nanoindentation to measure strain rate sensitivity focused on simple single phase metals such as nickel, or tungsten typically with nano-scale grains [28, 45, 46]. The technique we have used can be extended to measuring local rate sensitivity in industrially important multi-phase titanium alloys, provided that suitable assessment of the testing region is undertaken to ensure that tests are appropriately comparative and fair. This data is key as a first step in developing appropriate hypotheses towards a full understanding on how local microstructure controls dwell fatigue and failure of in-service components.

5. Conclusions

In this work we have demonstrated that the orientation and structure of colony titanium microstructures influences the strain rate sensitivity through careful use of nanoindentation testing. This testing strategy is relatively inexpensive and provides qualitative insight into the performance of complex microstructures, when combined with microstructural characterisation at an appropriate lengthscale (SEM, EBSD and FIB-SEM sectioning).

Indentation was performed at different strain rates in particular colonies to test the rate sensitivity of hard and soft colonies for these alloys. The two titanium alloys were heat treated to generate similar microstructures, with large colonies of similarly orientated α-laths connected by β-ligaments, contained within prior β grains. The tested volumes of α and β phases were from prior β grains, as they obeyed the BOR in all four cases.

Ti6242 has:

- a higher rate sensitivity (m=0.039) for the hard orientation when compared with the soft orientation (m=0.005)

- thin (0.3~0.4μm) β-ligaments connecting long straight α-laths (2.3~3.4μm wide)
- a β volume fraction of ~10%

Ti6246 has:

- comparable rate sensitivities for the hard and soft orientations (m=0.025)
- thin (0.7~0.8μm) β-ligaments connecting long straight α-laths (~1.0μm wide)
- a β volume fraction of ~45%

The nature of the difference in structural rate sensitivities for different alloys and different orientations was discussed. It is suggested that this is due to a combination of the thickness of the β lathes combined with the ability for slip to easily transfer across these complex microstructures. This is likely to have an impact when considering the effective structural unit when testing under complex loading regimes when rate sensitive effects are likely to play a significant role.

Supplementary online information

The individual indentation data associated with this article can be found in the online version at http://dx.doi.org/10.5281/zenodo.32145.

Acknowledgements

TSJ and TBB are grateful to the Engineering and Physical Science Research Council for funding through the HexMat programme grant EP/K034332/1 (for more information please see http://www.imperial.ac.uk/hexmat). TBB and DEJA would both like to acknowledge funding from the Royal Academy of Engineering Research Fellowship scheme. We would

also like to thank Professor Fionn Dunne (Imperial College) and Professor David Rugg (Rolls-Royce) for helpful discussions on dwell fatigue and strain rate sensitivity.

References

[1] M. Bache, A review of dwell sensitive fatigue in titanium alloys: the role of microstructure, texture and operating conditions, International journal of fatigue, 25 (2003) 1079-1087.
[2] W. Evans, M. Bache, Dwell-sensitive fatigue under biaxial loads in the near-alpha titanium alloy IMI685, International Journal of Fatigue, 16 (1994) 443-452.
[3] J. Qiu, Y. Ma, J. Lei, Y. Liu, A. Huang, D. Rugg, R. Yang, A Comparative Study on Dwell Fatigue of Ti-6Al-2Sn-4Zr-xMo (x= 2 to 6) Alloys on a Microstructure-Normalized Basis, Metallurgical and Materials Transactions A, 45 (2014) 6075-6087.
[4] F. Dunne, A. Walker, D. Rugg, A systematic study of hcp crystal orientation and morphology effects in polycrystal deformation and fatigue, in: Proceedings of the Royal Society of London A: Mathematical, Physical and Engineering Sciences, The Royal Society, 2007, pp. 1467-1489.
[5] A. Stroh, The formation of cracks as a result of plastic flow, in: Proceedings of the Royal Society of London A: Mathematical, Physical and Engineering Sciences, The Royal Society, 1954, pp. 404-414.
[6] F. Dunne, D. Rugg, A. Walker, Lengthscale-dependent, elastically anisotropic, physically-based hcp crystal plasticity: application to cold-dwell fatigue in Ti alloys, International Journal of Plasticity, 23 (2007) 1061-1083.
[7] G. Venkatramani, S. Ghosh, M. Mills, A size-dependent crystal plasticity finite-element model for creep and load shedding in polycrystalline titanium alloys, Acta materialia, 55 (2007) 3971-3986.
[8] F. Dunne, D. Rugg, On the mechanisms of fatigue facet nucleation in titanium alloys, Fatigue & Fracture of Engineering Materials & Structures, 31 (2008) 949-958.
[9] D. Davidson, D. Eylon, Titanium alloy fatigue fracture facet investigation by selected area electron channeling, Metallurgical Transactions A, 11 (1980) 837-843.
[10] W. Evans, The influence of microstructure on dwell sensitive fatigue in a near alpha titanium alloy, Scripta metallurgica, 21 (1987) 469-474.
[11] A. Pilchak, J. Williams, Observations of Facet Formation in Near-α Titanium and Comments on the Role of Hydrogen, Metallurgical and Materials Transactions A, 42 (2011) 1000-1027.
[12] V. Sinha, M. Mills, J.C. Williams, J. Spowart, Observations on the faceted initiation site in the dwell-fatigue tested Ti-6242 alloy: crystallographic orientation and size effects, Metallurgical and Materials Transactions A, 37 (2006) 1507-1518.
[13] E. Uta, N. Gey, P. Bocher, M. Humbert, J. Gilgert, Texture heterogeneities in αp/αs titanium forging analysed by EBSD-Relation to fatigue crack propagation, Journal of microscopy, 233 (2009) 451-459.
[14] T.B. Britton, H. Liang, F.P.E. Dunne, A.J. Wilkinson, The effect of crystal orientation on the indentation response of commercially pure titanium: experiments and simulations, P R Soc A, 466 (2010) 695-719.

[15] L. Wang, R.I. Barabash, Y. Yang, T.R. Bieler, M.A. Crimp, P. Eisenlohr, W. Liu, G.E. Ice, Experimental Characterization and Crystal Plasticity Modeling of Heterogeneous Deformation in Polycrystalline alpha-Ti, Metallurgical and Materials Transactions a-Physical Metallurgy and Materials Science, 42A (2011) 626-635.
[16] C. Zambaldi, Y.Y. Yang, T.R. Bieler, D. Raabe, Orientation informed nanoindentation of alpha-titanium: Indentation pileup in hexagonal metals deforming by prismatic slip, J Mater Res, 27 (2012) 356-367.
[17] T. Britton, F. Dunne, A. Wilkinson, On the mechanistic basis of deformation at the microscale in hexagonal close-packed metals, in: Proceedings of the Royal Society of London A: Mathematical, Physical and Engineering Sciences, The Royal Society, 2015, pp. 20140881.
[18] J.C. Gong, A.J. Wilkinson, Anisotropy in the plastic flow properties of single-crystal alpha titanium determined from micro-cantilever beams, Acta Mater, 57 (2009) 5693-5705.
[19] T.B. Britton, F.P.E. Dunne, A.J. Wilkinson, On the mechanistic basis of deformation at the microscale in hexagonal close-packed metals, P R Soc A, 471 (2015).
[20] J. Kwon, M.C. Brandes, P.S. Phani, A.P. Pilchak, Y.F. Gao, E.P. George, G.M. Pharr, M.J. Mills, Characterization of deformation anisotropies in an alpha-Ti alloy by nanoindentation and electron microscopy, Acta Mater, 61 (2013) 4743-4756.
[21] G.B. Viswanathan, E. Lee, D.M. Maher, S. Banerjee, H.L. Fraser, Direct observations and analyses alpha phase of an alpha/beta Ti-alloy of dislocation substructures in the formed by nanoindentation, Acta Mater, 53 (2005) 5101-5115.
[22] E. Merson, R. Brydson, A. Brown, The effect of crystallographic orientation on the mechanical properties of titanium, Journal of Physics: Conference Series, 126 (2008).
[23] D. Rugg, T. Britton, J. Gong, A. Wilkinson, P. Bagot, In-service materials support for safety critical applications–A case study of a high strength Ti-alloy using advanced experimental and modelling techniques, Materials Science and Engineering: A, 599 (2014) 166-173.
[24] W.C. Oliver, G.M. Pharr, Measurement of hardness and elastic modulus by instrumented indentation: Advances in understanding and refinements to methodology, Journal of materials research, 19 (2004) 3-20.
[25] X. Li, B. Bhushan, A review of nanoindentation continuous stiffness measurement technique and its applications, Materials characterization, 48 (2002) 11-36.
[26] J. Chen, Y. Shi, K. Lu, Strain rate sensitivity of a nanocrystalline Cu–Ni–P alloy, Journal of materials research, 20 (2005) 2955-2959.
[27] P. Huang, F. Wang, M. Xu, K. Xu, T. Lu, Dependence of strain rate sensitivity upon deformed microstructures in nanocrystalline Cu, Acta Materialia, 58 (2010) 5196-5205.
[28] V. Maier, K. Durst, J. Mueller, B. Backes, H.W. Höppel, M. Göken, Nanoindentation strain-rate jump tests for determining the local strain-rate sensitivity in nanocrystalline Ni and ultrafine-grained Al, Journal of Materials Research, 26 (2011) 1421-1430.
[29] J. Mueller, K. Durst, D. Amberger, M. Göken, Local investigations of the mechanical properties of ultrafine grained metals by nanoindentations, in: Materials Science Forum, Trans Tech Publ, 2006, pp. 31-36.
[30] Q. Wei, Strain rate effects in the ultrafine grain and nanocrystalline regimes—influence on some constitutive responses, Journal of materials science, 42 (2007) 1709-1727.
[31] J. Alkorta, J.M. Martínez-Esnaola, J. Gil Sevillano, Critical examination of strain-rate sensitivity measurement by nanoindentation methods: Application to severely deformed niobium, Acta Materialia, 56 (2008) 884-893.
[32] P. Cavaliere, Strain rate sensitivity of ultra-fine and nanocrystaline metals and alloys, Physica B: Condensed Matter, 403 (2008) 569-575.

[33] B. Lucas, W. Oliver, Indentation power-law creep of high-purity indium, Metallurgical and Materials Transactions A, 30 (1999) 601-610.
[34] M. Mayo, W. Nix, A micro-indentation study of superplasticity in Pb, Sn, and Sn-38 wt% Pb, Acta Metallurgica, 36 (1988) 2183-2192.
[35] J. Ye, Y. Wang, T. Barbee Jr, A. Hamza, Orientation-dependent hardness and strain rate sensitivity in nanotwin copper, Applied Physics Letters, 100 (2012) 261912.
[36] D. Peykov, E. Martin, R.R. Chromik, R. Gauvin, M. Trudeau, Evaluation of strain rate sensitivity by constant load nanoindentation, Journal of Materials Science, 47 (2012) 7189-7200.
[37] F. Wang, B. Li, T. Gao, P. Huang, K. Xu, T. Lu, Activation volume and strain rate sensitivity in plastic deformation of nanocrystalline Ti, Surface and Coatings Technology, 228 (2013) S254-S256.
[38] D. Chichili, K. Ramesh, K. Hemker, The high-strain-rate response of alpha-titanium: experiments, deformation mechanisms and modeling, Acta materialia, 46 (1998) 1025-1043.
[39] M. Meyers, G. Subhash, B. Kad, L. Prasad, Evolution of microstructure and shear-band formation in α-hcp titanium, Mechanics of Materials, 17 (1994) 175-193.
[40] T. Neeraj, D.-H. Hou, G. Daehn, M. Mills, Phenomenological and microstructural analysis of room temperature creep in titanium alloys, Acta materialia, 48 (2000) 1225-1238.
[41] R. Reed-Hill, C. Iswaran, M. Kaufman, A power law model for the flow stress and strain-rate sensitivity in CP titanium, Scripta metallurgica et materialia, 33 (1995) 157-162.
[42] G.E. Dieter, D. Bacon, Mechanical metallurgy, McGraw-Hill New York, 1986.
[43] G.M. Pharr, J.H. Strader, W. Oliver, Critical issues in making small-depth mechanical property measurements by nanoindentation with continuous stiffness measurement, Journal of Materials Research, 24 (2009) 653-666.
[44] K. Durst, V. Maier, Dynamic nanoindentation testing for studying thermally activated processes from single to nanocrystalline metals, Current Opinion in Solid State and Materials Science, (2015).
[45] V. Maier, A. Hohenwarter, R. Pippan, D. Kiener, Thermally activated deformation processes in body-centered cubic Cr–How microstructure influences strain-rate sensitivity, Scripta Materialia, (2015).
[46] V. Maier, C. Schunk, M. Göken, K. Durst, Microstructure-dependent deformation behaviour of bcc-metals–indentation size effect and strain rate sensitivity, Philosophical Magazine, (2014) 1-14.
[47] G.M. Pharr, E.G. Herbert, Y. Gao, The indentation size effect: A critical examination of experimental observations and mechanistic interpretations, Annual Review of Materials Research, 40 (2010) 271-292.
[48] S.J. Lloyd, A. Castellero, F. Giuliani, Y. Long, K.K. McLaughlin, J.M. Molina-Aldareguia, N.A. Stelmashenko, L.J. Vandeperre, W.J. Clegg, Observations of nanoindents via cross-sectional transmission electron microscopy: a survey of deformation mechanisms, P Roy Soc a-Math Phy, 461 (2005) 2521-2543.
[49] T.-S. Jun, G. Sernicola, F.P. Dunne, T.B. Britton, Local deformation mechanisms of two-phase Ti alloy, Materials Science and Engineering: A, 649 (2016) 39-47.
[50] W.C. Oliver, G.M. Pharr, An improved technique for determining hardness and elastic modulus using load and displacement sensing indentation experiments, Journal of materials research, 7 (1992) 1564-1583.
[51] T. Ferreira, W. Rasb, ImageJ user guide, (2012).
[52] W. Burgers, On the process of transition of the cubic-body-centered modification into the hexagonal-close-packed modification of zirconium, Physica, 1 (1934) 561-586.

[53] D. Bhattacharyya, G. Viswanathan, H.L. Fraser, Crystallographic and morphological relationships between β phase and the Widmanstätten and allotriomorphic α phase at special β grain boundaries in an α/β titanium alloy, Acta Materialia, 55 (2007) 6765-6778.
[54] D. He, J. Zhu, S. Zaefferer, D. Raabe, Y. Liu, Z. Lai, X. Yang, Influences of deformation strain, strain rate and cooling rate on the Burgers orientation relationship and variants morphology during β→ α phase transformation in a near α titanium alloy, Materials Science and Engineering: A, 549 (2012) 20-29.
[55] S. Suri, G. Viswanathan, T. Neeraj, D.-H. Hou, M. Mills, Room temperature deformation and mechanisms of slip transmission in oriented single-colony crystals of an α/β titanium alloy, Acta Materialia, 47 (1999) 1019-1034.
[56] J. Hedworth, M. Stowell, The measurement of strain-rate sensitivity in superplastic alloys, Journal of Materials Science, 6 (1971) 1061-1069.
[57] T. Kim, F. Dunne, Determination of superplastic constitutive equations and strain rate sensitivities for aerospace alloys, Proceedings of the Institution of Mechanical Engineers, Part G: Journal of Aerospace Engineering, 211 (1997) 367-380.
[58] T. Lee, J.H. Kim, S. Semiatin, C.S. Lee, Internal-variable analysis of high-temperature deformation behavior of Ti–6Al–4V: A comparative study of the strain-rate-jump and load-relaxation tests, Materials Science and Engineering: A, 562 (2013) 180-189.
[59] Q. Wei, S. Cheng, K. Ramesh, E. Ma, Effect of nanocrystalline and ultrafine grain sizes on the strain rate sensitivity and activation volume: fcc versus bcc metals, Materials Science and Engineering: A, 381 (2004) 71-79.
[60] D. Lunt, The effect of macrozones in Ti-6Al-4V on the strain localisation behaviour, in, University of Manchester, 2015.
[61] A.L. Pilchak, A simple model to account for the role of microtexture on fatigue and dwell fatigue lifetimes of titanium alloys, Scripta Materialia, 74 (2014) 68-71.
[62] D. Rugg, M. Dixon, F.E. Dunne, Effective structural unit size in titanium alloys, The Journal of Strain Analysis for Engineering Design, 42 (2007) 269-279.
[63] M. Savage, J. Tatalovich, M. Mills, Anisotropy in the room-temperature deformation of α–β colonies in titanium alloys: role of the α–β interface, Philosophical Magazine, 84 (2004) 1127-1154.
[64] M. Savage, J. Tatalovich, M. Zupan, K. Hemker, M. Mills, Deformation mechanisms and microtensile behavior of single colony Ti–6242Si, Materials Science and Engineering: A, 319 (2001) 398-403.
[65] F.P.E. Dunne, A. Walker, D. Rugg, A systematic study of hcp crystal orientation and morphology effects in polycrystal deformation and fatigue, P Roy Soc a-Math Phy, 463 (2007) 1467-1489.
[66] W.J. Evans, M.R. Bache, Dwell-Sensitive Fatigue under Biaxial Loads in the near-Alpha Titanium-Alloy Imi685, Int J Fatigue, 16 (1994) 443-452.
[67] J. Gong, A.J. Wilkinson, Anisotropy in the plastic flow properties of single-crystal α titanium determined from micro-cantilever beams, Acta Materialia, 57 (2009) 5693-5705.